

Interpretable pathological test for Cardio-vascular disease: Approximate Bayesian computation with distance learning

Ritabrata Dutta^{1*}, Karim Zouaoui-Boudjeltia², Christos Kotsalos³,
Alexandre Rousseau², Daniel Ribeiro de Sousa², Jean-Marc Desmet², Alain Van Meerhaeghe²,
Antonietta Mira⁴, Bastien Chopard³

¹ *University of Warwick, UK*

² *Université Libre de Bruxelles, CHU de Charleroi, Charleroi, Belgium*

³ *University of Geneva, Switzerland*

⁴ *Università della Svizzera italiana, Switzerland*

June 4, 2022

Abstract

Cardio/cerebrovascular diseases (CVD) have become one of the major health issue in our societies. But recent studies show that the present clinical tests to detect CVD are ineffectual as they do not consider different stages of platelet activation or the molecular dynamics involved in platelet interactions and are incapable to consider inter-individual variability. Here we propose a stochastic platelet deposition model and an inferential scheme for uncertainty quantification of these parameters using Approximate Bayesian Computation and distance learning. Finally we show that our methodology can learn biologically meaningful parameters, which are the specific dysfunctioning parameters in each type of patients, from data collected from healthy volunteers and patients. This work opens up an unprecedented opportunity of personalized pathological test for CVD detection and medical treatment. Also our proposed methodology can be used to other fields of science where we would need machine learning tools to be interpretable.

1 Introduction

Cardio/cerebrovascular diseases (CVD) were the first cause of mortality worldwide in 2015, causing 31% of deaths according to World Health Organization [Organization, 2015]. Blood platelets play a key role in the occurrence of these cardio/cerebrovascular accidents in addition to complex process of blood coagulation, involving adhesion, aggregation and spreading on the vascular wall to stop a hemorrhage while avoiding the vessel occlusion. Although, in a recent bio-medical evaluation study by Breet et al. [2010], the correlation between the clinical biological measures using platelet function tests and the occurrence of a cardiovascular event was found to be null for half of the techniques and rather modest for others, indicating the evident need for a more efficient tool or method to monitor patient platelet functionalities. This may be due to the fact that no current test allows the analysis of the different stages of platelet activation or the prediction of the in-vivo behavior of those platelets [Picker, 2011, Koltai et al., 2017]. In addition, the current clinical tests do not take into account the dynamic aspect of the process of platelet aggregation formation and the role that red blood cells can have in this process. To address these issues, Chopard et al. [2017b] provided a physical description of the adhesion and aggregation of platelets in the Impact-R device, by combining digital holography microscopy and mathematical modeling. They have developed a numerical model that quantitatively describes how platelets in a shear flow adhere and aggregate on a deposition surface. Further Dutta et al. [2018] showed how the five parameters of this model, specifying the deposition process and relevant for biomedical understanding of the phenomena, can be inferred from the blood sample collected from an individual using approximate Bayesian computation (ABC) [Lintusaari et al., 2017].

Our *main claim* here is that the values of some these parameters (eg. adhesion and aggregation rates) are precisely the information needed to assess various possible pathological situations and quantifying their severity regarding CVD.

Following this claim, we want to develop a methodology to identify medically interpretable parameters able to distinguish between patients and healthy. We point that this is in stark contrast to developing some data-based adhoc classification rule using Impact-R device data of patients for identification of new patients. To

*Corresponding author: Ritabrata.Dutta@warwick.ac.uk

develop such a pathological test interpretable to medical practitioners and scientists, we harness the strength of the machine learning algorithms to classify data between different patient types, through the extension of the stochastic platelet deposition model proposed in Chopard et al. [2017b] [Section 2.2] and ABC [Section 2.3] in conjunction with distance learning techniques [Suárez et al., 2018]. We note that the ABC inferential algorithms used for inferring the parameters in Dutta et al. [2018] are dependent on the choice of the discrepancy measures between dataset, which can be chosen via a distance learning approach from machine learning [Suárez et al., 2018, Weinberger and Saul, 2009] providing the most discriminant distance between dataset from different patient groups. Leveraging on this crucial link between ABC and distance learning [Pacchiardi et al., 2020], we develop a methodology to identify medically meaningful parameters, which are able to distinguish between different types of patients and also a way to estimate those parameters given the deposition patterns observed in the Impact-R of platelet collected for a patient. We further notice, the proposed approach can be applied patient per patient, in a systematic way, without the bias of a human operator.

Finally, to verify our claim and whether the proposed methodology provides us with a diagnostic tool for CVD, we perform an experiment divided into four stages: **1)** Collect blood or platelet from 24 patients (16 patients needing dialysis and 8 patients with Chronic Obstructive Pulmonary Disease (COPD) and 16 healthy volunteers; **2)** Study the deposition patterns observed in the Impact-R of platelet collected for each of the patients; **3)** Learn the distance from this dataset which is able to maximally distinguish between the 3 types of patients; **4)** Estimate the model parameters for each of the patients, using ABC with the use of the learned distance from Stage 3. Through this exercise we were able to identify medically meaningful parameters which are able to distinguish between patients of different types, opening up research directions in bio-medical arena to understand these processes and parameters better. The details of the validation of our methodology, experiments and our main findings are described in Section 3.

2 Model and Methods

Based on detailed *in vitro* experiments using the Impact-R device mimicking platelet adhesion-aggregation in blood vessels, first we provide a model which is an *in silico* counterpart for an in-depth description and understanding of the phenomenon and the underlying mechanisms.

2.1 Impact-R experiment

Impact-R [Shenkman et al., 2008], a well-known platelet function analyzer, is a cylindrical device whose bottom wall is a fixed disc (deposition substrate), while the upper wall is a rotating disc (shaped as a cone with a small angle) [Figure 1a]. The height of the device is 0.82 mm and due to the motion of the upper wall a pure shear flow is created. A controlled shear rate $\dot{\gamma}$ is produced in a given observation window of $1 \times 1\text{ mm}^2$, where we track the formation of clusters resulting from the deposition and aggregation of platelets. Blood was drawn from both healthy and diseased donors with different hematocrit (volume fraction of red blood cells (RBC)). Before starting the tests, a sample is recovered and analysed, to determine the concentration of activated (AP) and non-activated (NAP) platelets. Serum albumin, the most abundant protein in human blood plasma, antagonises with the platelets, preventing them from adhering to the substrate. The quantities of interest are the number of clusters and their size formed in the substrate, and the number of AP/NAP still in suspension. Our goal is to explain the observed (*in vitro* experiments) time evolution of the above quantities.

2.2 Stochastic Model of platelet deposition

This deposition process in Impact-R was successfully described with a mathematical model for the first time in Chopard et al. [2015], Chopard et al. [2017a] accounting for the following observations: (i) AP adhere to the deposition surface, forming a seed for a new cluster, (ii) NAP and AP can deposit at the periphery or on top of an existing cluster and (iii) Albumin (Al) deposits on the surface, thus reducing locally the adhesion and aggregation rates of platelets. A sketch of the situation shown in Figure 1b. In Chopard et al. [2017a], the platelets reach the bottom layer due to a RBC-enhanced shear-induced 1D diffusion. In the present work, we propose a fully stochastic model of platelet deposition, by substituting the 1D diffusion systems with a 3D random walk, while keeping the deposition dynamics the same. The reason of this new approach is to avoid the introduction of a boundary layer (denoted by Δz in Chopard et al. [2017a]) when coupling platelet transport with platelet deposition. With this particle based approach, a platelet becomes a candidate for deposition whenever it hits the deposition surface. In Chopard et al. [2017a] the diffusion coefficient D and the thickness of the boundary layer Δz were determined independently of the other model parameters. Now, instead of D and Δz two new parameters are considered, namely the characteristic velocities of activated and non-activated platelets. They will be inferred from the data, together with the adhesion and aggregation rates, and other quantities defined below.

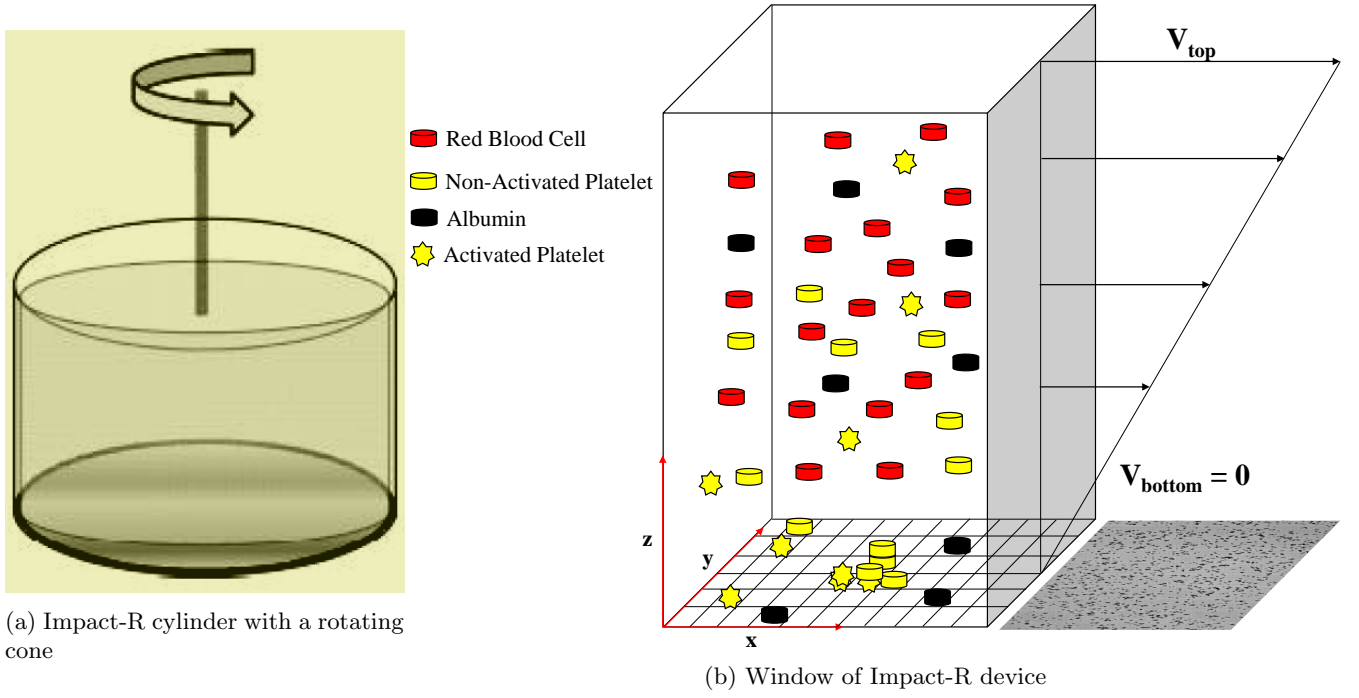


Figure 1: (a) **Impact-R** cylinder with a rotating cone to study the pattern of platelet deposition of a patient; (b) **Window of Impact-R**: The bottom wall is a fixed boundary of dimensions $1 \times 1 \text{ mm}^2$, the wall-bounded direction is 0.82 mm . The bulk contains whole blood at different hematocrit. The discretization of the substrate is such that in every cell can fit just one platelet. The initial densities of the blood particles are determined by the *in vitro* experiment and usually are about: $172 \text{ } 200 (\mu\text{l})^{-1}$ for NAP, $4808 (\mu\text{l})^{-1}$ for AP, $2.69 \times 10^{13} (\mu\text{l})^{-1}$ for Al. The image next to the discretised substrate corresponds to the *in vitro* experiment.

The random walk of the platelets can be described by their jump $(\Delta z(t), \Delta x(t), \Delta y(t))$ at each iteration t :

$$\Delta z(t) = \lambda v_z |s_z| dt, \quad (1)$$

$$\Delta x(t) = v_{xy} |s_{xy}| \cos(2\pi r) dt, \quad (2)$$

$$\Delta y(t) = v_{xy} |s_{xy}| \sin(2\pi r) dt, \quad (3)$$

where $v_{z,xy}$ is a speed unit, r is a random variable uniformly distributed in $[0, 1]$, $s_{z,xy} \in (-\infty, \infty)$ is a random variable distributed as a standard normal distribution, $\lambda \in \{-1, 1\}$ with probability $1/2$ for each outcome, and dt is the time step of the simulation. Superimposing the stochastic motion with the velocity field of the pure shear flow, the positions of the platelets are updated as

$$z_i(t + dt) = z_i(t) + \Delta z_i(t), \quad (4)$$

$$x_i(t + dt) = x_i(t) + \Delta x_i(t) + \dot{\gamma} z_i dt, \quad (5)$$

$$y_i(t + dt) = y_i(t) + \Delta y_i(t). \quad (6)$$

Owing to the different dynamics and physics governing the activated and non-activated platelets, they have in principle different speed units ($v_{z,xy}^{AP}, v_{z,xy}^{NAP}$). Regarding the motion of albumin, its abundance allows us to neglect the small density gradients due to its deposition, and thus albumin can deposit at any time at a maximum value of deposition rate.

The AP and NAP that cross the lower boundary of the computational domain are removed from the bulk if the deposition is successful, or get trapped at the Cell Free Layer (CFL) for a future deposition attempt (they never get re-injected into the bulk). Further, periodic conditions are applied at the x, y directions, and bounce back boundary condition for the platelets that cross the upper boundary. Assuming a good horizontal mixing in the xy -plane due to the rotating flow, and given its low impact on the deposition process, the stochastic part of the motion in the x, y directions can be fixed to the same order of magnitude as the z direction velocity. Therefore, we consider $v_{xy}^{AP} = v_z^{AP}$, $v_{xy}^{NAP} = v_z^{NAP}$ and $s_{xy} = s_z$.

Next we describe the deposition rates. Let us denote by $N_{i,j}(t)$ the number of candidate particles for deposition above the cell at position i, j of the discretised substrate. The deposition of the platelets and albumin on the substrate follow the stochastic rules described in Chopard et al. [2017a], i.e., based on the $N_{i,j}(t)$ and

on the occupancy of the i, j -th cell at time t . Albumin that reaches the substrate at time t deposits with a probability $P(t)$ which depends on the local density $\rho_{al}(t)$ of already deposited albumin. We assume that P is proportional to the remaining free space in the cell,

$$P(t) = p_F(\rho_{max} - \rho_{al}(t))dt, \quad (7)$$

where p_F is a parameter to be determined and ρ_{max} is given by the constraint that at most 100,000 albumin particles can fit in a deposition cell of area $\Delta S = 5 (\mu m)^2$, corresponding to the size of a deposited platelet (obtained as the smallest variation of cluster area observed with the microscope). An activated platelet that hits a platelet-free cell deposits with a probability Q , where Q decreases as the local concentration ρ_{al} of albumin increases. We assumed that

$$Q = p_{Ad} \exp(-a_T \rho_{al})dt, \quad (8)$$

where p_{Ad} and a_T are parameters to be determined. This expression can be justified by the fact that a platelet needs more free space than an albumin to attach to the substrate, due to their size difference. In other words, the probability of having enough space for a platelet, decreases roughly exponentially with the density of albumin in the substrate (more details in Chopard et al. [2017b]). In our model, AP and NAP can deposit next to already deposited platelets. From the above discussion, the aggregation probability R is assumed to be

$$R = p_{Ag} \exp(-a_T \rho_{al})dt, \quad (9)$$

with p_{Ag} another unknown parameter. We also introduce p_T the rate at which platelets deposit on top of an existing cluster. Figure 1b presents coarsely the competing adhesion-aggregation process between albumin and platelets. More details on the stochastic deposition rules can be found in Chopard et al. [2017a].

For the purpose of the present study, the platelet deposition model \mathcal{M} is parametrized in terms of the seven quantities introduced above, namely the adhesion rate p_{Ad} , the aggregation rates p_{Ag} and p_T , the deposition rate of albumin p_F , the attenuation factor a_T , and the velocities of AP and NAP v_z^{AP} and v_z^{NAP} . Collectively, we define

$$\boldsymbol{\theta} = (p_{Ag}, p_{Ad}, p_T, p_F, a_T, v_z^{AP}, v_z^{NAP}).$$

If the initial number of AP and NAP at time $t = 0$ ($\mathbb{N}_{platelet}(0)$ and $\mathbb{N}_{act-platelet}(0)$), as well as the concentration of albumin are known from the experiment, we can forward simulate the deposition of platelets over time using model \mathcal{M} for the given values of these parameters $\boldsymbol{\theta} = \boldsymbol{\theta}^*$:

$$\mathcal{M}[\boldsymbol{\theta} = \boldsymbol{\theta}^*] \rightarrow \{(\mathcal{S}_{agg-clust}(t), \mathbb{N}_{agg-clust}(t), \mathbb{N}_{platelet}(t), \mathbb{N}_{act-platelet}(t)), t = 0, \dots, T\}. \quad (10)$$

where $\mathcal{S}_{agg-clust}(t)$, $\mathbb{N}_{agg-clust}(t)$, $\mathbb{N}_{platelet}(t)$ and $\mathbb{N}_{act-platelet}(t)$ are correspondingly average size of the aggregation clusters, their number per mm^2 , the number of non-activated and pre-activated platelets per μl still in suspension at time t .

The Impact-R experiments have been repeated with the whole blood obtained from each of the volunteers and patients and the observations were made at time, 0 sec., 20 sec., 120 sec. and 300 sec. At these four time points, $(\mathcal{S}_{agg-clust}(t), \mathbb{N}_{agg-clust}(t), \mathbb{N}_{platelet}(t), \mathbb{N}_{act-platelet}(t))$ are measured. Let us call the observed dataset collected through experiment as,

$$\mathbf{x}^0 \equiv \{(\mathcal{S}_{agg-clust}^0(t), \mathbb{N}_{agg-clust}^0(t), \mathbb{N}_{platelet}^0(t), \mathbb{N}_{act-platelet}^0(t)) : t = 0 \text{ sec.}, \dots, 300 \text{ sec.}\}.$$

2.3 Estimation of model parameters

We can quantify the uncertainty of the parameter $\boldsymbol{\theta}$ by its posterior distribution $p(\boldsymbol{\theta}|\mathbf{x})$ given the observed dataset $\mathbf{x} = \mathbf{x}^0$. The posterior distribution is obtained by Bayes' theorem as $p(\boldsymbol{\theta}|\mathbf{x}^0) = \frac{\pi(\boldsymbol{\theta})p(\mathbf{x}^0|\boldsymbol{\theta})}{m(\mathbf{x}^0)}$, where $\pi(\boldsymbol{\theta})$, $p(\mathbf{x}^0|\boldsymbol{\theta})$ and $m(\mathbf{x}^0) = \int \pi(\boldsymbol{\theta})p(\mathbf{x}^0|\boldsymbol{\theta})d\boldsymbol{\theta}$ are, correspondingly, the prior distribution on the parameter $\boldsymbol{\theta}$, the likelihood function, and the marginal likelihood. If the likelihood function could be evaluated, at least up to a normalizing constant, then the posterior distribution could be approximated by drawing a representative sample of parameter values from it using (Markov chain) Monte Carlo sampling schemes [Robert and Casella, 2005]. Unfortunately, the likelihood function induced by the platelets deposition model is analytically intractable. In this setting, approximate Bayesian computation (ABC) [Lintusaari et al., 2017] offers a way to sample from an approximate posterior distribution and opens up the possibility of sound statistical inference of the parameter $\boldsymbol{\theta}$.

Approximate Bayesian computation (ABC) The fundamental ABC rejection sampling scheme iterates the following steps:

1. Draw $\boldsymbol{\theta}$ from the prior $\pi(\boldsymbol{\theta})$.
2. Simulate a synthetic dataset \mathbf{x}^{sim} from the simulator-based model $\mathcal{M}(\boldsymbol{\theta})$.
3. Accept the parameter value $\boldsymbol{\theta}$ if $d(\mathbf{x}^{\text{sim}}, \mathbf{x}^0) < \epsilon$. Otherwise, reject $\boldsymbol{\theta}$.

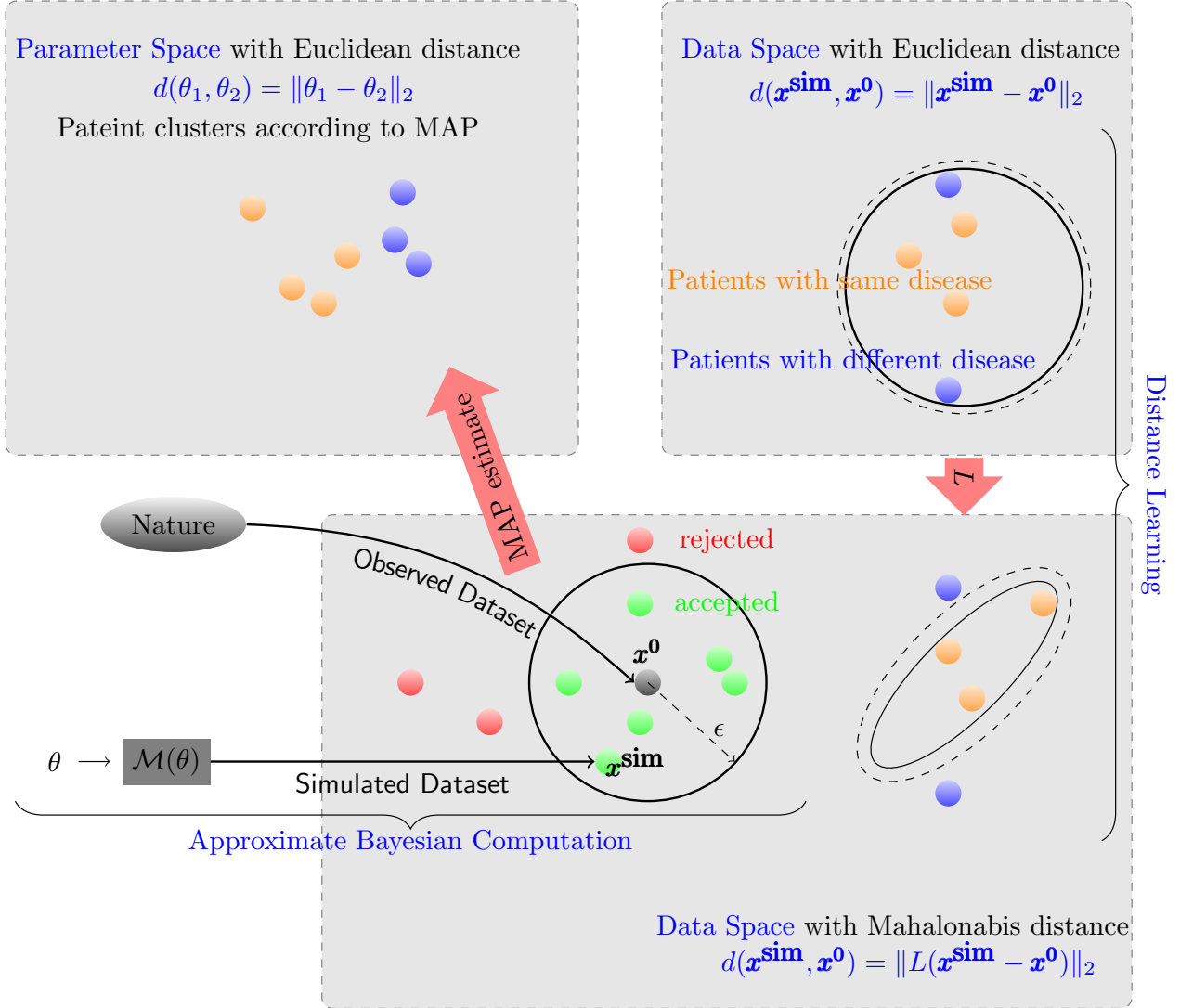


Figure 2: **ABC in conjunction with Distance learning: Distance learning:** We first learn a distance $d(\mathbf{x}_1, \mathbf{x}_2) = \|L(\mathbf{x}_1 - \mathbf{x}_2)\|_2$ between the dataset from patients which is able to discriminate between patients of different types better. **Approximate Bayesian computation:** Then having observed data \mathbf{x}^0 from an individual patient (the gray dot), we sample parameter values and generate observations through the simulator, that are then accepted (green) or rejected (red) according to their distance from the observation. The visualization is in a 2-dimensional data space. **Maximum a posteriori estimate:** Finally, using the posterior samples produced by ABC we compute the MAP estimates of the parameters of the model for each patient, which is able to tell us which parameters are significantly different between different types of patients.

See Figure 2 for a visualization of the above algorithm.

Here, the metric on the dataspace $d(\mathbf{x}^{\text{sim}}, \mathbf{x}^0)$ measures the closeness between \mathbf{x}^{sim} and \mathbf{x}^0 . The accepted $(\theta, \mathbf{x}^{\text{sim}})$ pairs are thus jointly sampled from a distribution proportional to $\pi(\theta)p_{d,\epsilon}(\mathbf{x}^0|\theta)$, where $p_{d,\epsilon}(\mathbf{x}^0|\theta)$ is an approximation to the likelihood function $p(\mathbf{x}^0|\theta)$:

$$p_{d,\epsilon}(\mathbf{x}^0|\theta) = \int p(\mathbf{x}^{\text{sim}}|\theta) \mathbb{K}_\epsilon(d(\mathbf{x}^{\text{sim}}, \mathbf{x}^0)) d\mathbf{x}^{\text{sim}}, \quad (11)$$

where $\mathbb{K}_\epsilon(d(\mathbf{x}^{\text{sim}}, \mathbf{x}^0))$ is in this case a probability density function proportional to $\mathbb{1}(d(\mathbf{x}^{\text{sim}}, \mathbf{x}^0) < \epsilon)$ ¹. Besides

¹ $\mathbb{1}(\cdot)$ is used as an indicator function.

this choice for $\mathbb{K}_\epsilon(d(\mathbf{x}^{\text{sim}}, \mathbf{x}^0))$, that has been exploited in several ABC algorithms (for instance Beaumont [2010], Drovandi and Pettitt [2011], Del Moral et al. [2012], Lenormand et al. [2013]), ABC algorithms relying on different choices exist, for instance being proportional to $\exp(-d(\mathbf{x}^{\text{sim}}, \mathbf{x}^0)/\epsilon)$ in simulated-annealing ABC (SABC) [Albert et al., 2015]. More advanced algorithms than the simple rejection scheme detailed above are possible, for instance ones based on Sequential Monte Carlo [Del Moral et al., 2012, Lenormand et al., 2013], in which various parameter-data pairs are considered at a time and are evolved over several generations, while ϵ is decreased towards 0 at each generation to improve the approximation of the likelihood function, so that you are able to approximately sample from the true posterior distribution. For the inference of parameters of the platelets deposition model, here we choose the adaptive population Monte Carlo approximate Bayesian computation (APMCABC) algorithm, proposed in Lenormand et al. [2013], based on its suitability to high performance computing systems [Dutta et al., 2017b]. For practical implementation, APMCABC was run for 30 iterations generating 3500 samples from the posterior distribution of the model parameters given data from each patient, keeping all other parameters fixed to the default values proposed in Python package ‘abcpv’ [Dutta et al., 2017a]. Next we explain, how the distance between datasets used for ABC was chosen via a distance learning approach and finally how the maximum a posteriori estimates (MAP) of the parameters computed.

Data-driven distance learning (DL) Traditionally, distance between \mathbf{x}^{sim} and \mathbf{x}^0 are defined by considering Euclidean distance between simulated and observed dataset. When the data \mathbf{x} is high-dimensional, a common practice in ABC literature is to define d as Euclidean distance between a lower-dimensional summary statistics $S : \mathbf{x}^{\text{sim}} \mapsto S(\mathbf{x}^{\text{sim}})$. Reducing the data to suitably chosen summary statistics may also yield more robust inference with respect to noise in the data. Moreover, if the statistics is sufficient, then the above modification provides us with a consistent posterior approximation [Didelot et al., 2011], meaning that we are still guaranteed to converge to the true posterior distribution in the limit $\epsilon \rightarrow 0$. As sufficient summary statistics are not known for most of the complex models, the choice of summary statistics remains a problem [Csilléry et al., 2010] and they have been previously chosen in a problem-specific manner [Blum et al., 2013, Fearnhead and Prangle, 2012, Gutmann et al., 2018].

As the main goal of the present research is to be able to learn parameter values which are able to differentiate between different patient types, here we propose to use the distance measure which is able to differentiate data from different patient groups. This setup falls under a well-developed field of research in metric-learning [Suárez et al., 2018], which has recently been used to learn the distances for ABC [Pacchiardi et al., 2020]. We use Large Margin Nearest Neighbor Metric Learning (LMNN) [Weinberger and Saul, 2009], to learn a Mahalanobis distance between data from any two patients \mathbf{x}_1 and \mathbf{x}_2 ,

$$d_M(\mathbf{x}_1, \mathbf{x}_2) = \sqrt{(\mathbf{x}_1 - \mathbf{x}_2)^T M (\mathbf{x}_1 - \mathbf{x}_2)} \quad (12)$$

where M is a $d \times d$ positive semi-definite matrix. We note that learning of the Mahalanobis distance case corresponds to learning a transformation of the data. It is sufficient to recall that for each positive semidefinite matrix M there exists a square matrix L such that $M = L^T L$. Therefore, we can write Equation 12 in the following way:

$$d_M(\mathbf{x}_1, \mathbf{x}_2) = \sqrt{(\mathbf{x}_1 - \mathbf{x}_2)^T L^T L (\mathbf{x}_1 - \mathbf{x}_2)} = \sqrt{(L(\mathbf{x}_1 - \mathbf{x}_2))^T L(\mathbf{x}_1 - \mathbf{x}_2)} = \|L(\mathbf{x}_1 - \mathbf{x}_2)\|_2, \quad (13)$$

from which it is clear that the above corresponds to learning the transformation $\mathbf{x} \mapsto L\mathbf{x}$ which is able to cluster data from different patient groups and then computing the Euclidean distance between the transformed data. To learn the transformation, LMNN solves the following optimization problem:

$$\min_L \sum_{ij} \eta_{ij} \|L(\mathbf{x}_i - \mathbf{x}_j)\|^2 + \sum_{ijl} \eta_{ij}(1 - y_{ij}) [1 + \|L(\mathbf{x}_i - \mathbf{x}_j)\|^2 + \|L(\mathbf{x}_i - \mathbf{x}_l)\|^2]_+, \quad (14)$$

where \mathbf{x}_i is a data from a patient, \mathbf{x}_j is one of its k -nearest neighbors from the same type of patients, and \mathbf{x}_l are all the other data from patients of different type within the neighborhood, $\eta_{ij}, y_{ij} \in \{0, 1\}$ are indicators, $\eta_{ij} = 1$ represents \mathbf{x}_j is one of the k -nearest neighbors (same type of patient) of \mathbf{x}_i , $y_{ij} = 0$ indicates $\mathbf{x}_i, \mathbf{x}_j$ are different types of patients, $[\cdot]_+ = \max(0, \cdot)$ is the Hinge loss. Intuitively, LMNN tries to learn a metric which keeps k -nearest neighbors from the same patient group closer, while keeping patients from different groups separated by a large margin. Further we note LMNN does not make any assumptions about the distribution of the data. For the practical implementation, we chose $k = 6$ while keeping all other tuning parameters to the default values as provided in Python package ‘metric-learn’ [De Vazelhes et al., 2020].

Maximum a posteriori estimate (MAP) Given an observed dataset \mathbf{x}^0 , we want to estimate the corresponding θ . APMCABC inference scheme provides us with Z samples $(\theta_i)_{i=1}^Z$ from the posterior distribution $p(\theta|\mathbf{x}^0)$ given the data for each patient. We consider a smooth approximation of the marginal posterior distribution (given data for a specific patient) of the parameters using Gaussian kernel density estimator with a

bandwidth chosen by Silverman's rule [Silverman, 1986] and compute the mode of the smoothed marginal posterior distribution using quasi-Newton method of Broyden, Fletcher, Goldfarb, and Shanno (BFGS) [page 136 of Nocedal and Wright [2006]] as the estimate of parameters for each specific patient. This estimate will be considered as the maximum a posteriori estimate (MAP) of the parameters. The Gaussian kernel density and BFGS algorithm were used as implemented in Python package 'scipy' [Virtanen et al., 2020].

3 Results and Discussion

Dataset: To validate our claim, we have analyzed data collected from healthy volunteers (Group 1), patients needing dialysis (Group 2) or patients affected by Chronic Obstructive Pulmonary Disease (COPD) (Group 3). We were able to recruit 16 volunteers and 16 patients correspondingly for Group 1 and 2 and 8 COPD patients for Group 3 and collect their blood sample for testing. Half of the 16 patients having dialysis were also patients of diabetes and the volunteers and patients were chosen from a broad age group, such that the collected data was representative enough.

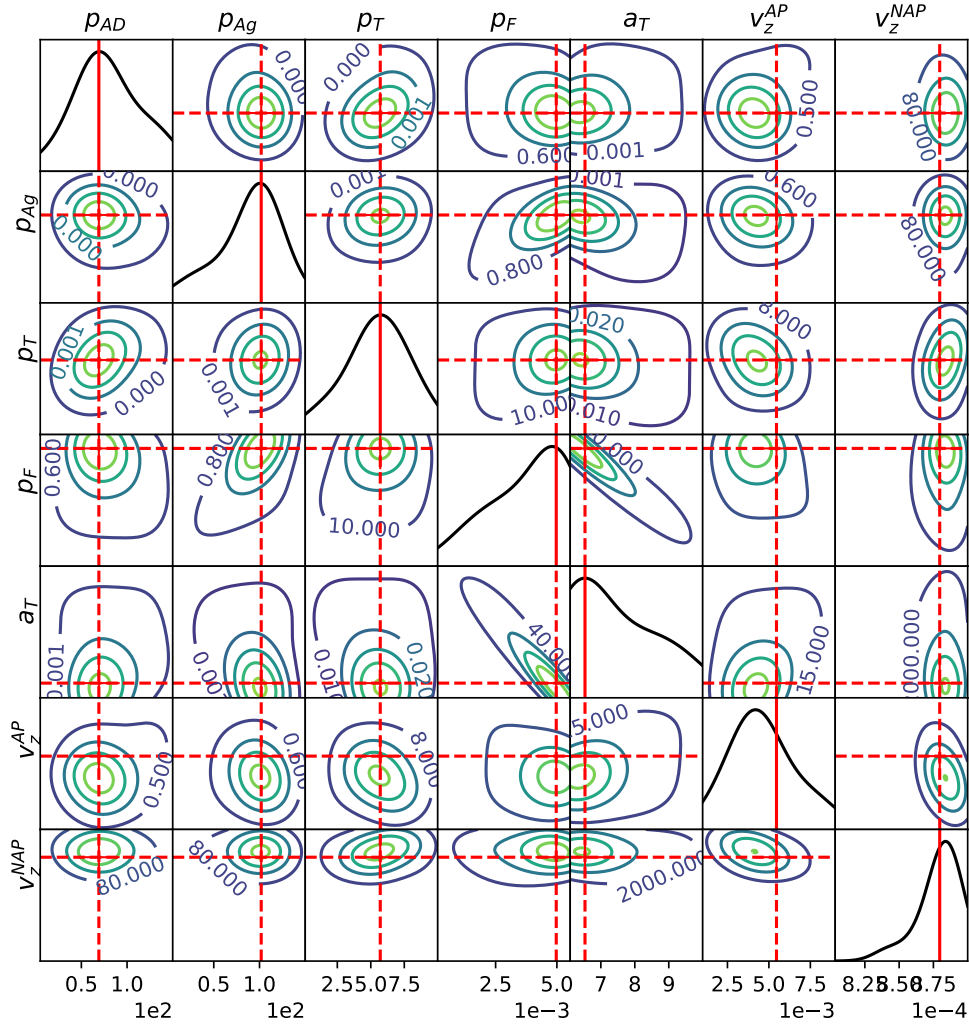


Figure 3: Posterior distribution for a COPD patient, where the red cross indicates the MAP estimate of the parameters p_{AD} [s^{-1}], p_{Ag} [s^{-1}], p_T [s^{-1}], p_F [s^{-1}], a_T [$\mu m^2 s^{-1}$], v_z^{AP} [ms^{-1}], v_z^{NAP} [ms^{-1}].

Inference of parameters: First we learn a projection of the dataset to a 2-dimensional space using LMNN, where different types of patients can be differentiated through clustering. Although we notice that the two features defining this two-dimensional space, do not have a meaningful representation in biology as they are just linear combinations of the observed time-series of the platelet deposition pattern. Next, the Euclidean distance on this projection space is used for ABC to infer the parameters of the stochastic platelets depositions model for each of the volunteers (or patients), using the corresponding deposition and aggregation pattern of the platelets in their blood displayed in Impact-R machine. This provides us with a posterior distribution of the parameters given the data from each individual volunteer (patient). In Figure 3, we illustrate the inferred posterior distribution for a randomly chosen patient with COPD and the corresponding MAP estimate of the parameters.

Kruskal-Wallis H-test: To test whether the patient specific estimated parameters of the model can distinguish patients from healthy volunteers and between different types of the patients, we use the Kruskal-Wallis H-test [Kruskal and Wallis, 1952] which assumes the null hypothesis that the population median of all of the different types of patients are equal. The computed test statistics and p-values between all the three groups (healthy volunteers, patients needing dialysis and patients with COPD) are reported in the column 1 of Table 1. Considering a cutoff for significance of 0.05, the null hypothesis gets rejected for the parameters p_{Ad} , p_{Ag} , v_z^{AP} and v_z^{NAP} indicating the values of these parameters significantly differ between the groups.

Parameters	All three classes	Healthy vs Dialysis	Healthy vs COPD	Dialysis vs COPD
p_{Ad}	7.26 (0.02)	7.36 (0.006)	0.84 (0.35)	1.35 (0.24)
p_{Ag}	7.79 (0.02)	6.76 (0.009)	3.84, (0.05)	0.09 (0.75)
p_T	3.52 (0.17)	0.06 (0.79)	2.53 (0.11)	3.15 (0.07)
p_F	2.19 (0.33)	0.62 (0.42)	0.45 (0.5)	2.34 (0.12)
a_T	0.75 (0.68)	0.36 (0.54)	0.003 (0.95)	0.84 (0.35)
v_z^{AP}	4.98 (0.08)	4.61 (0.03)	0.45 (0.5)	1.65 (0.19)
v_z^{NAP}	7.40 (0.02)	6.56 (0.01)	0.84 (0.35)	2.73 (0.09)

Table 1: Statistics (P-values) of Kruskal-Wallis test using maximum a posteriori (MAP) estimates of the parameters. Here three classes Healthy, Dialysis and COPD stands for healthy volunteers, patients under dialysis and patients with COPD.

	Healthy	Dialysis	COPD
Healthy	-	$p_{Ad}, p_{Ag}, v_z^{AP}, v_z^{NAP}$	p_{Ag}
Dialysis	$p_{Ad}, p_{Ag}, v_z^{AP}, v_z^{NAP}$	-	p_T, v_z^{NAP}
COPD	p_{Ag}	p_T, v_z^{NAP}	-

Table 2: Discriminatory parameters.

We notice that the rejection of the null hypothesis does not indicate which of these groups differ. Hence, we perform post-hoc Kruskal-Wallis H-test between healthy volunteers vs patients needing dialysis and patients with COPD and between patients needing dialysis and patients with COPD [columns 2, 3 and 4 of Table 1 respectively]. This indicates that the p_{Ag} can differentiate both type of patients needing dialysis and having COPD from the healthy volunteers, in addition to the p_{Ad} being able to differentiate patients needing dialysis from healthy volunteers. Further we notice that for the parameters p_T and v_z^{NAP} , the Kruskal-Wallis H-test provides a p-value above but very close to the cutoff for significance 0.05 indicating their possible capability in distinguishing between patients needing dialysis and having COPD. The not optimal performance in the ability to distinguish COPD patients both from the healthy volunteers and patients needing dialysis probably can be explained by observing that we have 50% less number of COPD patients than other types in our dataset. We list the parameters which are capable to distinguish between the corresponding groups in Table 2. Further the distinguishing capability of these parameters can be illustrated through the boxplots of the distribution of the estimated parameters values in each of the three groups in Figure 4.

Discriminating parameters: The most discriminating parameters according to our analysis are p_{Ad} , p_{Ag} , v_z^{AP} and v_z^{NAP} [Table 2 and Figure 4]. Further, these four parameters can be divided into two distinct functional categories:

First category consisting of p_{Ad} and p_{Ag} represents intrinsic changes in platelets associated with the presence of pathology. The common thread between dialysis patients and COPD patients is the existence of chronic systemic inflammation implicated in the development of cardiovascular disease. In response to inflammation, it is well known that platelets in COPD and dialysis patients are activated in the bloodstream, altering their

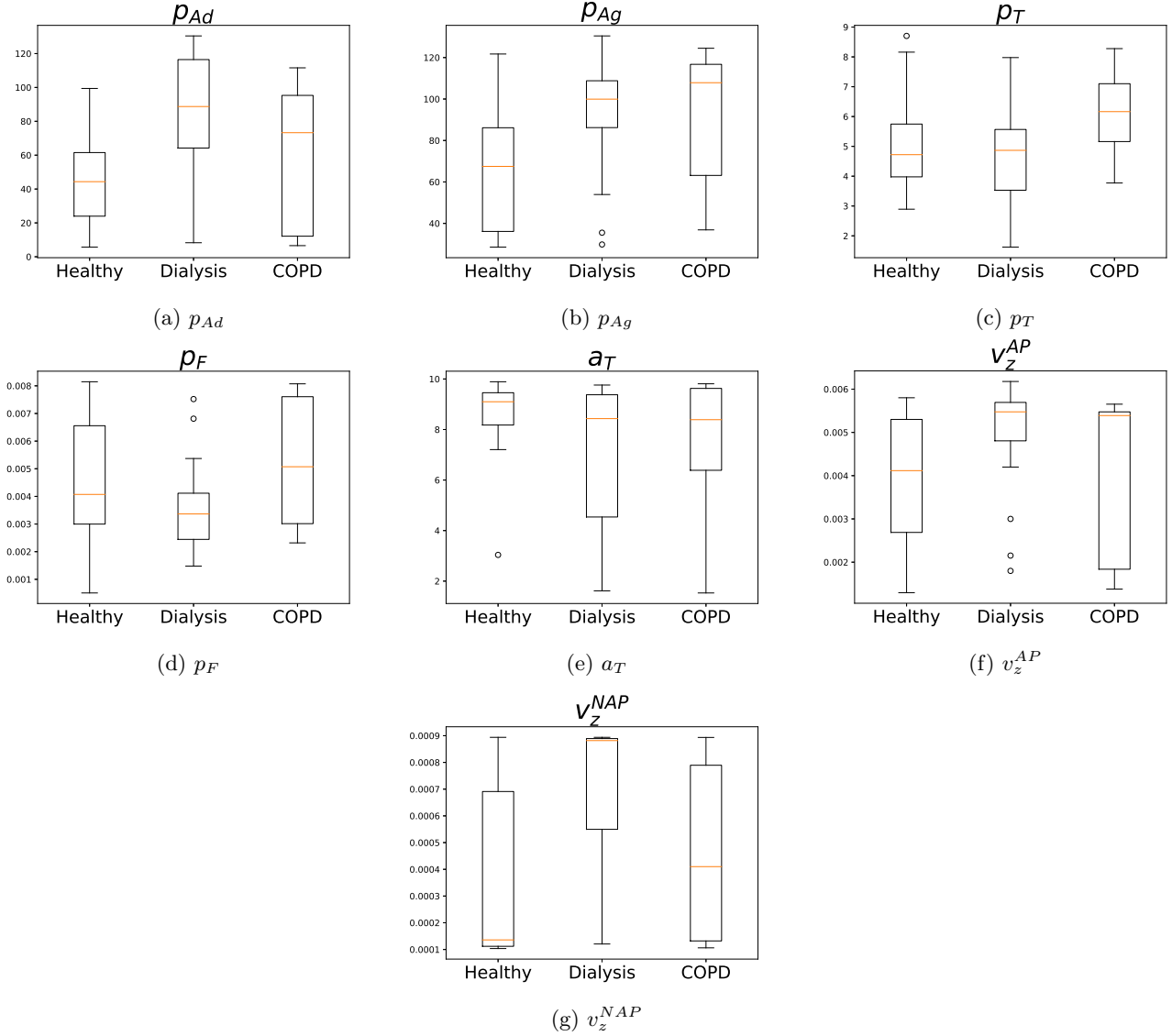


Figure 4: Boxplot of estimated parameter values clustered according to patient types. HV: Healthy volunteers (16 patients); Dialysis: All Patients having dialysis (16 patients); COPD: Patients with COPD (8 patients)

hemostatic properties [Mourikis et al., 2020, Thijs et al., 2008, Mallah et al., 2020, Malerba et al., 2016] and therefore the process of adhesion and aggregation.

Second category consisting of v_z^{AP} and v_z^{NAP} reflect another aspect of the presence of pathology. Various studies have demonstrated significant interactions between red blood cells (RBCs) and platelets in the blood-stream. These interactions lead, among others, to the phenomenon of platelet margination: in the blood flow, platelets globally migrate toward the wall of the blood vessel. Furthermore, in pathological situations, RBCs may undergo biochemical and conformational changes, altering blood rheology [Bujak et al., 2015]. Spherization of RBCs has been demonstrated in sepsis, dialysis patients, COPD patients and other pathologies causing chronic or acute systemic inflammation [Piagnerelli et al., 2007, Zouaoui Boudjeltia et al., 2020]. Recently, we reported that the RBC spherization induces an increase in platelet adhesion and aggregation processes. The numerical simulations provide one explanation of the experimental results obtained, indicating that the RBC spherization causes an increase in platelet transport to the wall, which. [Zouaoui Boudjeltia et al., 2020]. This indicates that the changes of RBC shapes affect platelets transport and thus the platelets properties of adhesion and aggregation to the wall.

4 Conclusion

We propose a stochastic model explaining platelet deposition in Impact-R device and a methodology using distance learning and approximate Bayesian computation to learn meaningful biological parameters which differentiates between different types of patients. To our knowledge, both the modeling and methodology proposed in this paper is novel.

Finally, we collect platelet deposition patterns from patients and healthy volunteers and analyse them using the proposed methodology, which was able to reveal the most important properties of the platelets that are dysfunctioning in each of these patient categories. This opens up new doors for platelets functioning tests and medical treatments. We also notice that the use of ABC in conjunction with distance learning can be applied to other fields of science where we would like to have an interpretable machine learning method.

Author contribution

RD, BC and KZ designed the research, CK, BC and RD developed the stochastic model, RD developed the methodology for distance learning and approximate Bayesian computation, RD conducted the inference, KZ provided medical expertise in developing methodology, AR have done Platelets and RBCs counting and cytometry analysis, DRS have done Impact-R experiments and analysis, JD and AVM selected and recruited patients in dialysis and COPD correspondingly, AM helped in computation, RD, BC, KZ wrote the paper.

Funding and Acknowledgment

This project has received funding from the European Union’s Horizon 2020 research and innovation programme under grantagreement No 823712 (CompBioMed2 project). We also acknowledge support from the Swiss National Supercomputing Centre (CSCS, Piz-Daint supercomputer) and the HPC Facilities of the University of Geneva (Baobab cluster). All the codes and dataset used for this research, can be downloaded from StochasticPlatelets-DepositionCode.

References

- C. Albert, R. K. Hans, and A. Scheidegger. A simulated annealing approach to approximate Bayesian computations. *Statistics and Computing*, 25:1217–1232, 2015.
- M. A. Beaumont. Approximate bayesian computation in evolution and ecology. *Annual review of ecology, evolution, and systematics*, 41:379–406, 2010.
- M. G. Blum, M. A. Nunes, D. Prangle, S. A. Sisson, and others. A comparative review of dimension reduction methods in approximate Bayesian computation. *Statistical Science*, 28(2):189–208, 2013.
- N. J. Breet, J. W. van Werkum, H. J. Bouman, J. C. Kelder, H. J. Ruven, E. T. Bal, V. H. Deneer, A. M. Harmsze, J. A. van der Heyden, B. J. Rensing, et al. Comparison of platelet function tests in predicting clinical outcome in patients undergoing coronary stent implantation. *Jama*, 303(8):754–762, 2010.
- K. Bujak, J. Wasilewski, T. Osadnik, S. Jonczyk, A. Kołodziejska, M. Gierlotka, and M. Gasior. The prognostic role of red blood cell distribution width in coronary artery disease: a review of the pathophysiology. *Disease markers*, 2015, 2015.
- B. Chopard, D. Ribeiro de Sousa, J. Latt, F. Dubois, C. Yourassowsky, P. Van Antwerpen, O. Eker, L. Vanhamme, D. Perez-Morga, G. Courbebaisse, and K. Zouaoui Boudjeltia. A physical description of the adhesion and aggregation of platelets. *ArXiv e-prints*, 2015.
- B. Chopard, D. R. de Sousa, J. Lätt, L. Mountrakis, F. Dubois, C. Yourassowsky, P. Van Antwerpen, O. Eker, L. Vanhamme, D. Perez-Morga, et al. A physical description of the adhesion and aggregation of platelets. *Royal Society Open Science*, 4(4):170219, 2017a.
- B. Chopard, D. R. de Sousa, J. Lätt, L. Mountrakis, F. Dubois, C. Yourassowsky, P. Van Antwerpen, O. Eker, L. Vanhamme, D. Perez-Morga, et al. A physical description of the adhesion and aggregation of platelets. *Royal Society open science*, 4(4):170219, 2017b.
- K. Csilléry, M. G. Blum, O. E. Gaggiotti, and O. François. Approximate Bayesian computation (ABC) in practice. *Trends in Ecology & Evolution*, 25(7):410–418, 2010.

- W. De Vazelhes, C. Carey, Y. Tang, N. Vauquier, and A. Bellet. metric-learn: Metric learning algorithms in python. *Journal of Machine Learning Research*, 21(138):1–6, 2020.
- P. Del Moral, A. Doucet, and A. Jasra. An adaptive sequential monte carlo method for approximate bayesian computation. *Statistics and Computing*, 22(5):1009–1020, 2012.
- X. Didelot, R. G. Everitt, A. M. Johansen, D. J. Lawson, and others. Likelihood-free estimation of model evidence. *Bayesian Analysis*, 6(1):49–76, 2011.
- C. C. Drovandi and A. N. Pettitt. Estimation of parameters for macroparasite population evolution using approximate bayesian computation. *Biometrics*, 67(1):225–233, 2011.
- R. Dutta, M. Schoengens, J. Onnela, and A. Mira. Abcpy: A user-friendly, extensible, and parallel library for approximate bayesian computation. In *Proceedings of the Platform for Advanced Scientific Computing Conference*. ACM, June 2017a.
- R. Dutta, M. Schoengens, A. Ummadisingu, J.-P. Onnela, and A. Mira. Abcpy: A high-performance computing perspective to approximate bayesian computation. *arXiv preprint arXiv:1711.04694*, 2017b.
- R. Dutta, B. Chopard, J. Lätt, F. Dubois, K. Zouaoui Boudjeltia, and A. Mira. Parameter estimation of platelets deposition: Approximate bayesian computation with high performance computing. *Frontiers in physiology*, 9: 1128, 2018.
- P. Fearnhead and D. Prangle. Constructing summary statistics for approximate Bayesian computation: semi-automatic approximate Bayesian computation [with Discussion]. *Journal of the Royal Statistical Society. Series B (Statistical Methodology)*, 74(3):419–474, 2012. ISSN 1369-7412.
- M. U. Gutmann, R. Dutta, S. Kaski, and J. Corander. Likelihood-free inference via classification. *Statistics and Computing*, 28(2):411–425, 2018.
- K. Koltai, G. Kesmarky, G. Feher, A. Tibold, and K. Toth. Platelet aggregometry testing: Molecular mechanisms, techniques and clinical implications. *International journal of molecular sciences*, 18(8):1803, 2017.
- W. H. Kruskal and W. A. Wallis. Use of ranks in one-criterion variance analysis. *Journal of the American statistical Association*, 47(260):583–621, 1952.
- M. Lenormand, F. Jabot, and G. Deffuant. Adaptive approximate bayesian computation for complex models. *Computational Statistics*, 28(6):2777–2796, 2013.
- J. Lintusaari, M. U. Gutmann, R. Dutta, S. Kaski, and J. Corander. Fundamentals and recent developments in approximate bayesian computation. *Systematic biology*, 66(1):e66–e82, 2017. doi: 10.1093/sysbio/syw077. URL <https://doi.org/10.1093/sysbio/syw077>.
- M. Malerba, A. Olivini, A. Radaeli, F. L. M. Ricciardolo, and E. Clini. Platelet activation and cardiovascular comorbidities in patients with chronic obstructive pulmonary disease. *Current medical research and opinion*, 32(5):885–891, 2016.
- H. Mallah, S. Ball, J. Sekhon, K. Parmar, and K. Nugent. Platelets in chronic obstructive pulmonary disease: An update on pathophysiology and implications for antiplatelet therapy. *Respiratory Medicine*, page 106098, 2020.
- P. Mourikis, C. Helten, L. Dannenberg, T. Hohlfeld, J. Stegbauer, T. Petzold, B. Levkau, T. Zeus, M. Kelm, and A. Polzin. Platelet reactivity in patients with chronic kidney disease and hemodialysis. *Journal of Thrombosis and Thrombolysis*, 49(1):168–172, 2020.
- J. Nocedal and S. J. Wright. Numerical optimization. new york city. *Springer-Verlag*. doi, 10:978–0, 2006.
- W. H. Organization. <http://www.who.int/mediacentre/factsheets/fs317/en/>, 2015.
- L. Pacchiardi, P. Künzli, M. Schoengens, B. Chopard, and R. Dutta. Distance-learning for approximate bayesian computation to model a volcanic eruption. *Sankhya B*, pages 1–30, 2020.
- M. Piagnerelli, K. Z. Boudjeltia, D. Brohée, A. Vereerstraeten, P. Piro, J.-L. Vincent, and M. Vanhaeverbeek. Assessment of erythrocyte shape by flow cytometry techniques. *Journal of clinical pathology*, 60(5):549–554, 2007.
- S. Picker. In-vitro assessment of platelet function. *Transfus Apher Sci*, 44:305–19, 2011.

- C. P. Robert and G. Casella. *Monte Carlo Statistical Methods*. Springer-Verlag New York, Inc., 2005.
- B. Shenkman, Y. Einav, O. Salomon, D. Varon, and N. Savion. Testing agonist-induced platelet aggregation by the impact-r [cone and plate (let) analyzer (cpa)]. *Platelets*, 19(6):440–446, 2008.
- B. W. Silverman. *Density estimation for statistics and data analysis*, volume 26. CRC press, 1986.
- J. L. Suárez, S. García, and F. Herrera. A tutorial on distance metric learning: Mathematical foundations, algorithms and software. *arXiv preprint arXiv:1812.05944*, 2018.
- A. Thijs, P. Nanayakkara, P. Ter Wee, P. Huijgens, C. Van Guldener, and C. Stehouwer. Mild-to-moderate renal impairment is associated with platelet activation: a cross-sectional study. *Clinical nephrology*, 70(4):325, 2008.
- P. Virtanen, R. Gommers, T. E. Oliphant, M. Haberland, T. Reddy, D. Cournapeau, E. Burovski, P. Peterson, W. Weckesser, J. Bright, S. J. van der Walt, M. Brett, J. Wilson, K. J. Millman, N. Mayorov, A. R. J. Nelson, E. Jones, R. Kern, E. Larson, C. J. Carey, Í. Polat, Y. Feng, E. W. Moore, J. VanderPlas, D. Laxalde, J. Perktold, R. Cimrman, I. Henriksen, E. A. Quintero, C. R. Harris, A. M. Archibald, A. H. Ribeiro, F. Pedregosa, P. van Mulbregt, and SciPy 1.0 Contributors. SciPy 1.0: Fundamental Algorithms for Scientific Computing in Python. *Nature Methods*, 17:261–272, 2020. doi: 10.1038/s41592-019-0686-2.
- K. Q. Weinberger and L. K. Saul. Distance metric learning for large margin nearest neighbor classification. *Journal of Machine Learning Research*, 10(2), 2009.
- K. Zouaoui Boudjeltia, C. Kotsalos, D. R. de Sousa, A. Rousseau, C. Lelubre, O. Sartenaer, M. Piagnerelli, J. Dohet-Eraly, F. Dubois, N. Tasiaux, et al. Spherization of red blood cells and platelet margination in copd patients. *Annals of the New York Academy of Sciences*, 2020.